Supplementary Information (SI) for ChemComm.
This journal is © The Royal Society of Chemistry 2026

*Electronic Supplementary Information (ESI)*

# Copper phyllosilicate and $CeO_2$ integrated catalyst for the rapid catalytic transfer hydrogenation of furfural to furfuryl alcohol

Huabo Li,[a,b] Yanfei Zhang,[b] Deyuan Ji,[b] Yingfeng Cheng,[b] Songlin Wang,[b] Lei Zhang,[a] and Yang Zeng*[,c]

[a] *College of Environmental and Chemical Engineering, Chongqing Three Gorges University, Chongqing 404020, P. R. China*

[b] *School of Chemistry and Chemical Engineering, Henan Institute of Science and Technology, Xinxiang 453003, Henan Province, P. R. China*

[c] *School of Material Science and Engineering, Chongqing Jiaotong University, Chongqing 400074, P. R. China*

**Corresponding author.*

*E-mail: yzeng@cqjtu.edu.cn. (Y. Zeng)*

# 1 Experimental

## 1.1 Materials

Cerium nitrate hexahydrate (Aldrich, 99.5%), copper nitrate trihydrate (Aldrich, 99.99%), sodium hydroxide (Aldrich, 99%) hexadecyl trimethyl ammonium bromide (CTAB, Aldrich, 99%), tetraethyl orthosilicate (TEOS, Aldrich, 99%), ammonia solution (Aldrich, 28% in $H_2O$), furfural (FF, Aldrich, 99%), furfuryl alcohol (FOL, Aldrich, 98%), 5-hydroxymethyl-2-furaldehyde (5-HMF, Aldrich, 99.5%), isopropanol (*i*-PrOH, Aldrich, 99.9%), methanol (Aldrich, 99.9%), and ethanol (Aldrich, 99.9%) were used as received without further purification. Deionized water was produced by using an ultrapure water system.

## 1.2 Catalysts preparation

*Synthesis of $CeO_2$.* $CeO_2$ was synthesized according to a previous literature.[1] Typically, 6.292 g $Ce(NO_3)_3 \cdot 6H_2O$ was dissolved in 30 mL of deionized water with continuous stirring to obtain solution A. 58.0 g of NaOH was dissolved in 90 mL of deionized water to obtain solution B. Solution A was added dropwise into solution B under continuous stirring, and the resulted mixture was aged at room temperature for 2 h. The mixture was transferred into a 200 mL Teflon-lined stainless-steel autoclave. Subsequently, hydrothermal treatment was carried out at 373 K for 24 h. After cooling to room temperature, the product was washed several times with deionized water until the pH of the filtrate was neutral. The obtained powder was dried in an oven at 393 K for 12 h and calcined in static air at 623 K for 4 h at a ramping rate of 2 K $min^{-1}$. The as-obtained powder was denoted as $CeO_2$ for use.

*Synthesis of $CeO_2$@$SiO_2$.* 1.0 g CTAB was dissolved in a 110 mL ethanol solution (20 vol.% ethanol in water), and 0.5 g $CeO_2$ was ultrasonically dispersed in the solution for 1 h. Aqueous ammonia was added to adjust the pH to 11. 2.5 vol.% TEOS in ethanol solution was added dropwise through a syringe pump, the solution was continuously stirred at room temperature for 12 h to ensure complete hydrolysis of TEOS. The samples were washed alternately with deionized water and ethanol several times to remove the excess CTAB. The as-obtained sample was dried in an oven at 393 K overnight.

*Synthesis of xCuPs/$CeO_2$ catalyst.* The as-obtained $CeO_2$@$SiO_2$ was ultrasonically dispersed in 100 mL deionized water for 30 min. Subsequently, 0.510 g $Cu(NO_3)_2 \cdot 3H_2O$ was dissolved, and the pH was adjusted to 10-11 by aqueous ammonia.

The mixture was continuously aged for 3 h, and transferred to a Teflon-lined autoclave for a hydrothermal reaction at 473 K for 12 h, and then naturally cooled down to room temperature. The precipitate was filtrated and washed with ethanol and deionized water, respectively. The as-obtained sample was dried in an oven at 393 K overnight, and calcined in a muffle under static air at 623 K for 4 h with a ramping rate of 5 K $min^{-1}$. The as-prepared catalyst was denoted as 10CuPs/$CeO_2$. To further regulate the catalyst structure, the copper loadings were adjusted, and the obtained catalysts were recorded as 15CuPs/$CeO_2$, 20CuPs/$CeO_2$, 25CuPs/$CeO_2$, and 30CuPs/$CeO_2$, respectively.

*Synthesis of CuPs+$CeO_2$ and Cu/$CeO_2$ catalysts.* The CuPs was fabricated via an ammonia-evaporation hydrothermal method reported in our previous work.[2] The physically mixed CuPs+$CeO_2$ catalyst was prepared by milling CuPs and $CeO_2$ powders in a mortar to investigate the effect of the composite on catalytic performance. The Cu/$CeO_2$ catalyst was synthesized by using the impregnation method. The procedure was as follows: 2.0 g of $CeO_2$ was uniformly dispersed in 100 mL of deionized water. Then, 1.901 g of $Cu(NO_3)_2 \cdot 3H_2O$ was added to the suspension and stirred until dissolved. Subsequently, 0.2 mol $L^{-1}$ $Na_2CO_3$ solution was slowly dropped until the pH was 11 under vigorous stirring. The mixed solution was placed in a 353 K water bath and continuously stirred for 1.5 h. After the impregnation, the product was filtered and washed with deionized water to remove impurities. The obtained sample was dried at 373 K and then calcined at 723 K in static air for 4 h with a ramping rate of 5 K $min^{-1}$. The resulting sample was labeled as Cu/$CeO_2$ catalyst.

## 1.3 Characterizations

The composition and phase of the as-prepared catalysts were analyzed using an X-ray Powder diffractometer (D8 Advance, Bruker) at a voltage of 40 kV and a current of 40 mA, with Cu K$\alpha$ radiation as the excitation source. The 2$\theta$ scanning range was set between 10° and 90°, with a speed of 5° $min^{-1}$. The crystallite size was calculated using the Scherrer equation:

$$D = \frac{K\lambda}{\beta \cos\theta}$$

Where $D$ represents the crystallite size, $K$ is the Scherrer constant (typically taken as 0.87), $\lambda$ denotes the X-ray wavelength, $\beta$ refers to the full width at half maximum (FWHM) of the diffraction peak, and $\theta$ is the Bragg diffraction angle.

The morphology was observed using a field emission transmission electron microscope (Tecnai G2 F20, FEI) at an accelerating voltage of 120 kV. The samples

were ultrasonically dispersed in ethanol for 5 minutes. The suspension was then dropped onto a carbon-coated nickel grid for observation. HAADF imaging mode was utilized to visualize smaller nanoparticles. Particle size distribution (PSD) was determined by measuring approximately 100 particles from the images, enabling the calculation of the average particle size.

$N_2$ adsorption-desorption isotherms, specific surface area, pore size distribution, and pore volume of the samples were determined using an automated physical adsorption analyzer (Tristar II 3020, Micromeritics). Before measurement, the samples were degassed under $N_2$ atmosphere at 573 K for 3 h. Subsequently, $N_2$ adsorption-desorption experiments were conducted at 77 K. Specific surface areas were calculated using the Brunauer–Emmett–Teller (BET) method, while pore size distributions were derived based on the Barrett–Joyner–Halenda (BJH) model.

The bulk elemental composition of the samples was determined via ICP-OES with an optical emission spectrometer (Agilent 5110). Solid samples were dissolved in acid and left overnight at room temperature. The solutions were filtered and properly diluted for analysis.

Fourier transform infrared spectroscopy (FT-IR) was conducted using an FT-IR spectrometer (Tensor 27, Bruker) equipped with a DTGS detector. The samples were mixed with KBr, pressed into self-supporting pellets, and scanned over the wavenumber range of 4000–400 $cm^{-1}$ at a resolution of 4 $cm^{-1}$. Each spectrum was scanned 32 times.

The reduction behaviors of the samples were evaluated using a chemisorption analyzer (AutoChem 2950 HP, Micromeritics). About 30 mg of sample was loaded into a U-shaped quartz tube and pretreated by heating from room temperature to 473 K at a ramping rate of 10 K $min^{-1}$ under a continuous Ar flow (50 mL $min^{-1}$) for 1 h. After cooling to 313 K, the system was exposed to a 10 vol.% $H_2$/Ar flow (50 mL $min^{-1}$) for 30 min until the baseline was stabilized. The sample was reduced to 923 K at 10 K $min^{-1}$, and hydrogen consumption was monitored using a thermal conductivity detector (TCD). The corresponding peak area ($A_1$) was recorded. The sample was cooled to room temperature, purged with high-purity argon for 30 minutes, then heated to 333 K and exposed to a $N_2O$/Ar flow (50 mL $min^{-1}$) to oxidize surface copper species. Subsequently, the sample was purged with Ar flow for 30 min to remove physically adsorbed $N_2O$. Finally, the system was switched to 10 vol.% $H_2$/Ar and stabilized for 30 min before repeating the temperature-programmed reduction to 923 K. The hydrogen uptake peak area ($A_2$) was recorded. The dispersion and metallic copper

surface area were calculated as follows:

$$D_{Cu} = \frac{2A_1}{A_1} \times 100\%$$

$$S_{Cu}\ (m^2\ g_{Cu}^{-1}) = \frac{D_{Cu} \times N_{av}}{M_{Cu} \times 1.46 \times 10^{19}}$$

Where $N_{av}$ is the Avogadro constant = $6.02 \times 10^{23}$ mol$^{-1}$; $M_{Cu}$: relative atomic mass = 63.5 g mol$^{-1}$.

The X-ray photoelectron spectroscopy (XPS) analysis was performed on an X-ray photoelectron spectrometer (ESCALAB 250XI, Thermo Scientific) with monochromatic Al K$\alpha$ radiation ($hv$ = 1486.6 eV) served as the excitation source. The Auger excited spectroscopy (XAES) of Cu LMM was also collected. The obtained spectra were referenced to the C 1*s* peak at 284.6 eV from contaminated carbon. The XPS and XAES data were deconvolution fitted by the XPSPEAK 4.1 software.

Raman spectra were collected with a Raman spectrometer (DXR2, Thermo Scientific). The Excitation source was a 532 nm laser, and spectral resolution was maintained at 1.8 cm$^{-1}$.

Pyridine adsorption infrared spectroscopy (Py-IR) was performed using a Thermo Scientific Nicolet 380 FT-IR spectrometer to explore the acidic properties. Before adsorption, samples were reduced at 573 K for 1 h and then cooled to 298 K for background measurement. Pyridine vapor was introduced at 298 K for 1 h, followed by evacuation to eliminate weakly adsorbed species. The spectra were recorded at 298 K and 413 K with 16 times scanning.

The $^{1}$H and $^{13}$C nuclear magnetic resonance (NMR) spectra were recorded on an Avance NEO instruments (Bruker) to identify the products from the CTH reaction of biomass-derived molecules. The reaction mixture was separated by centrifugation. The solution was evaporated under reduced pressure, and the residue was purified using silica gel column chromatography (hexane/ethyl acetate, 8:2). The $^{1}$H NMR and $^{13}$C NMR spectra were acquired at 400 MHz and 100 MHz, respectively, using $CDCl_3$ as the solvent.

## 1.4 DFT calculation

Ab initio calculations were performed with the periodic density functional theory (DFT) code Vienna ab initio simulation package (VASP).[3] The exchange and correlation energy was calculated within the generalized gradient approximation (GGA) using the Perdew−Burke−Ernzerhof (PBE) functional.[4] To include van der Waals forces, the D3 correction was added as implemented by Grimme et al.[5] The electron-core

interaction was described with the projector augmented wave (PAW) method.[6] The electronic wave functions were expanded using a plane wave basis set with an energy cutoff of 400 eV. The Cu(111) model was developed to represent the $Cu^0$ sites, and the $Cu/SiO_2$ and $Cu/SiO_2/CeO_2$ models were configured and optimized with [$SiO_4$] layer on the $CeO_2$ surface to form Cu–O–Si and C–O–Ce interfaces. All structures were relaxed until the residual forces on the free atoms were smaller than 0.02 eV/Å. Geometry optimizations were carried out using Gamma type k-point meshes of 1 × 1 × 1.

The adsorption energies ($E_{ads}$) of molecules (*i*-PrOH and FF) on the surface were calculated according to

$$E_{\text{ads}} = E_{\text{total}} - E_{\text{mol}} - E_{\text{sur}}$$

Where, $E_{mol}$, $E_{total}$, and $E_{sur}$ are the DFT calculated energies of molecules and metal surfaces with and without molecules adsorbed.

Furthermore, Atomic Simulation Environment (ASE) package[7] and VESTA[8] were employed to aid the model building.

## 1.5 Catalytic evaluation

The catalytic transfer hydrogenation of FF to produce FOL was carried out in a commercial high-pressure reactor system supplied by Xi'an Taikang Biotechnology Co., Ltd. The experimental procedure was as follows: 50 mg of the catalyst was placed into a tube furnace and activated under a 5 vol.% $H_2$/Ar atmosphere. Next, 1 mmol of FF, 20 mL of *i*-PrOH, and the pre-reduced catalyst were added to a polytetrafluoroethylene (PTFE) liner. After the liner was sealed in the reactor, the atmosphere inside was purged with argon for several times to guarantee the inert conditions, and then pressurized to 2.0 MPa. The reaction was conducted at 413 K with a stirring rate of 650 rpm for 2 h. The liquid product was collected following centigrade separation and then analyzed on a Fuli GC 9790PLUS gas chromatograph equipped with a flame ionization detector (FID) through a SGE Analytical Science capillary column (30 m × 0.32 mm × 0.5 μm). *n*-Butanol was employed as the internal standard for accurate quantification. The conversion and yield were calculated using the following equations:

$$Con._{\text{FF}}(\%) = \frac{n_{\text{FF-in}} - n_{\text{FF-out}}}{n_{\text{FF-in}}} \times 100\%$$

$$Sel._{\text{FOL}}(\%) = \frac{n_{\text{FOL}}}{n_{\text{FF-in}} - n_{\text{FF-out}}} \times 100\%$$

$$Yield_{\text{FOL}}(\%) = Con._{\text{FF}} \times Sel._{\text{FOL}}$$

Where, $n_{FF\text{-}in}$ is the initial mole number of the FF, $n_{FF\text{-}out}$ is the mole number of the FF after reaction, and $n_{FOL}$ is the mole number of the FOL after reaction. Since FOL and 2-MeF were identified as the primary products of CTH, only small amounts of other by-products were detected. Thus, the other products have not been clarified in detail, include the etherification product derived from FOL and *i*-PrOH, as well as an acetal formed from acetalization of aldehyde as an intermediate which further generate the ether product.[9]

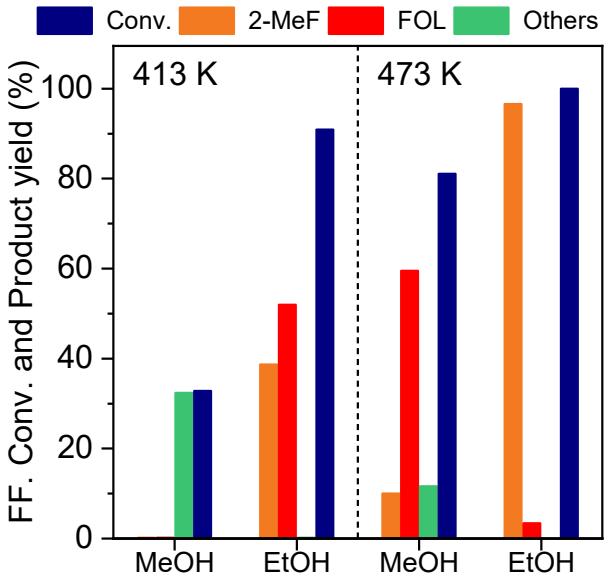


**Fig. S1** FF CTH performance over the integrated 25CuPs/$CeO_2$ catalyst in methanol and ethanol solvents, respectively. Reaction conditions: $m_{cat.}$ = 50 mg, $T$ = 413 K & 473 K, $t$ = 2 h, $n$(FF) = 1 mmol, $V_{i\text{-PrOH}}$ = 20 mL, $P$(Ar) = 2 MPa.

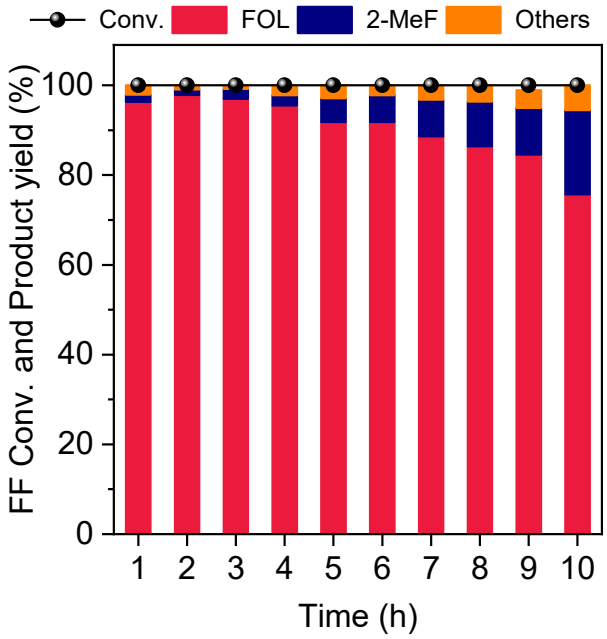


**Fig. S2** FF CTH performance over the integrated 25CuPs/$CeO_2$ catalyst as a function of reaction time. Reaction conditions: $m_{cat.}$ = 50 mg, $T$ = 413 K, $n$(FF) = 1 mmol, $V_{i\text{-PrOH}}$ = 20 mL, $P$(Ar) = 2 MPa.

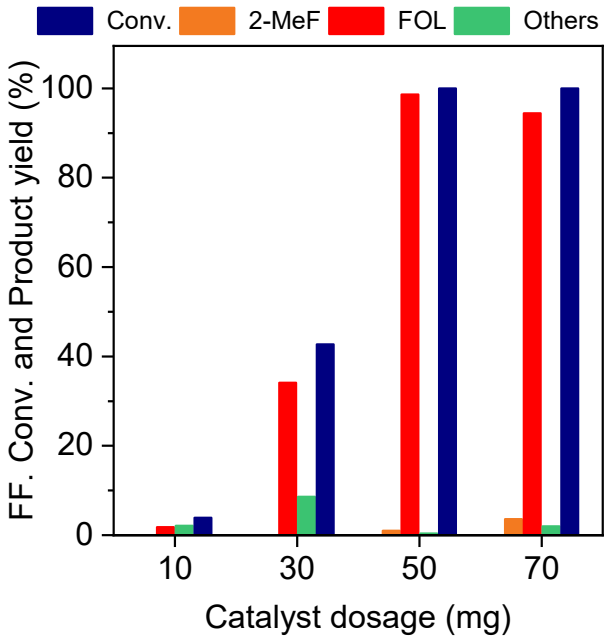


**Fig. S3** FF CTH performance over the integrated 25CuPs/$CeO_2$ catalyst with different catalyst dosage. Reaction conditions: $T$ = 413 K, $t$ = 2 h, $n$(FF) = 1 mmol, $V_{i\text{-PrOH}}$ = 20 mL, $P$(Ar) = 2 MPa.

When the catalyst dosage was 10 mg, small amount of FF was converted. The 25CuPs/$CeO_2$ catalyst afforded a furfuryl alcohol (FOL) yield of 35% at an FF conversion of 43%, while the catalyst dosage was increased to 30 mg. The optimal catalytic performance was attained at a catalyst loading of 50 mg, reaching a maximum FOL yield of 98.6%. However, the deep hydrogenation occurred at a dosage of 70 mg, leading to the increase of the by-product 2-methylfuran (2-MeF) in the solution. These results further confirmed that appropriate catalyst dosage is important for achieving high FOL selectivity, as both prolonged reaction time and excessive catalyst dosage promote the deep hydrogenation and reduce the catalytic selectivity.

**Table S1** Catalytic transfer hydrogenation performance of the biomass derived carbonyl components over the 25CuPs/$CeO_2$ catalyst.

| Substrate | Main product | Temperature (K) | Time (h) | Conversion (%) | Yield (%) |
|---|---|---|---|---|---|
| 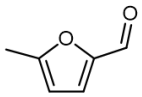 | 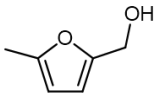 | 413 | 12 | >99 | 95 |
| 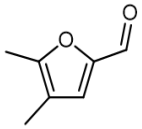 | 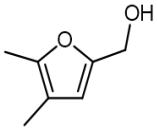 | 413 | 12 | >99 | 93 |
| 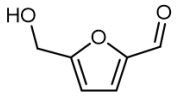 | 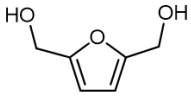 | 373 | 10 | 87 | 82 |
| 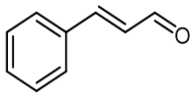 | 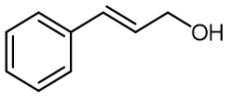 | 453 | 12 | 85 | 78 |
| 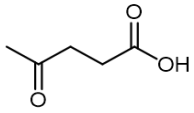 | 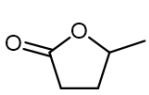 | 433 | 12 | >99 | 85 |

Reaction conditions: $m_{cat.}$ = 50 mg, $V_{i\text{-PrOH}}$ = 20 mL, $n_{substrate}$ = 1 mmol.

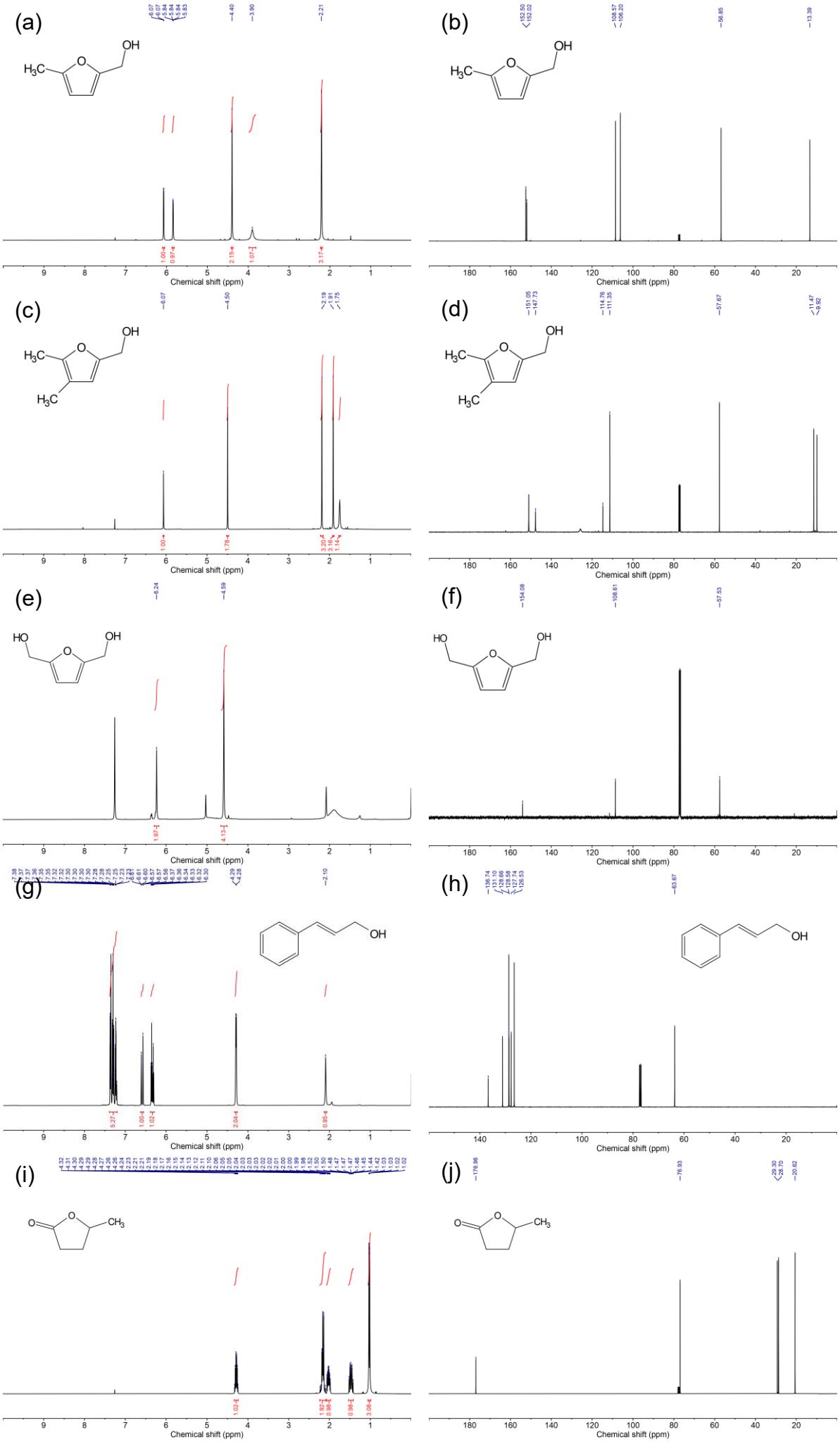
(a)
(b)
(c)
(d)
(e)
(f)
(g)
(h)
(i)
(j)
Chemical shift (ppm)

**Fig. S4** $^{1}$H NMR spectra of the products 5-methyl-2-furanmethanol (a), 4,5-dimethyl-2-furanmethanol (c), 2,5-furandimethanol (e), cinnamyl alcohol (g), γ-valerolactone (i). $^{13}$C NMR spectra of the products 5-methyl-2-furanmethanol (b), 4,5-dimethyl-2-furanmethanol (d), 2,5-furandimethanol (f), cinnamyl alcohol (h), γ-valerolactone (j)

*5-Methyl-2-furanmethanol*, $^{1}$H NMR (400 MHz, $CDCl_3$) $\delta$ 6.07 (d, $J$ = 3.2 Hz, 1H), 5.87 – 5.81 (m, 1H), 4.40 (s, 2H), 3.90 (s, 1H), 2.21 (s, 3H) ppm. $^{13}$C NMR (100 MHz, $CDCl_3$) $\delta$ 152.50, 152.02, 108.57, 106.20, 56.85, 13.39 ppm.

*4,5-Dimethyl-2-furanmethanol*, $^{1}$H NMR (400 MHz, $CDCl_3$) $\delta$ 6.07 (s, 1H), 4.50 (s, 2H), 2.19 (s, 3H), 1.91 (s, 3H), 1.75 (bs, 1H) ppm. $^{13}$C NMR (100 MHz, $CDCl_3$) $\delta$ 151.05, 147.73, 114.76, 111.35, 57.67, 11.47, 9.92 ppm.

*2,5-Furandimethanol*, $^{1}$H NMR (400 MHz, $CDCl_3$) $\delta$ 6.24 (s, 2H), 4.59 (s, 4H) ppm. $^{13}$C NMR (100 MHz, $CDCl_3$) $\delta$ 154.08, 108.61, 57.53 ppm.

*Cinnamyl alcohol*, $^{1}$H NMR (400 MHz, $CDCl_3$) $\delta$ 7.39 – 7.20 (m, 5H), 6.59 (dt, $J$ = 15.8, 1.6 Hz, 1H), 6.34 (dt, $J$ = 15.9, 5.7 Hz, 1H), 4.29 (d, $J$ = 5.4 Hz, 2H), 2.10 (s, 1H) ppm. $^{13}$C NMR (100 MHz, $CDCl_3$) $\delta$ 136.74, 131.10, 128.66, 128.58, 127.74, 126.53, 63.67 ppm.

*γ-Valerolactone*, $^{1}$H NMR (400 MHz, $CDCl_3$) $\delta$ 4.28 (dp, $J$ = 7.8, 6.3 Hz, 1H), 2.24 – 2.09 (m, 2H), 2.02 (dddd, $J$ = 13.4, 8.4, 6.5, 5.2 Hz, 1H), 1.53 – 1.42 (m, 1H), 1.06 – 0.99 (m, 3H) ppm. $^{13}$C NMR (100 MHz, $CDCl_3$) $\delta$ 176.96, 76.93, 29.30, 28.70, 20.62 ppm.

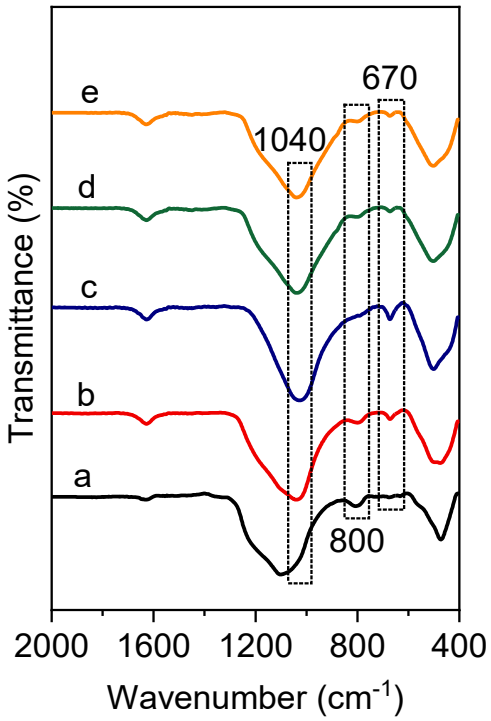


**Fig. S5** FT-IR spectra of the as-calcined *x*CuPs/$CeO_2$ catalysts: (a) $x = 10$, (b) $x = 15$, (c) $x = 20$, (d) $x = 25$, (e) $x = 30$.

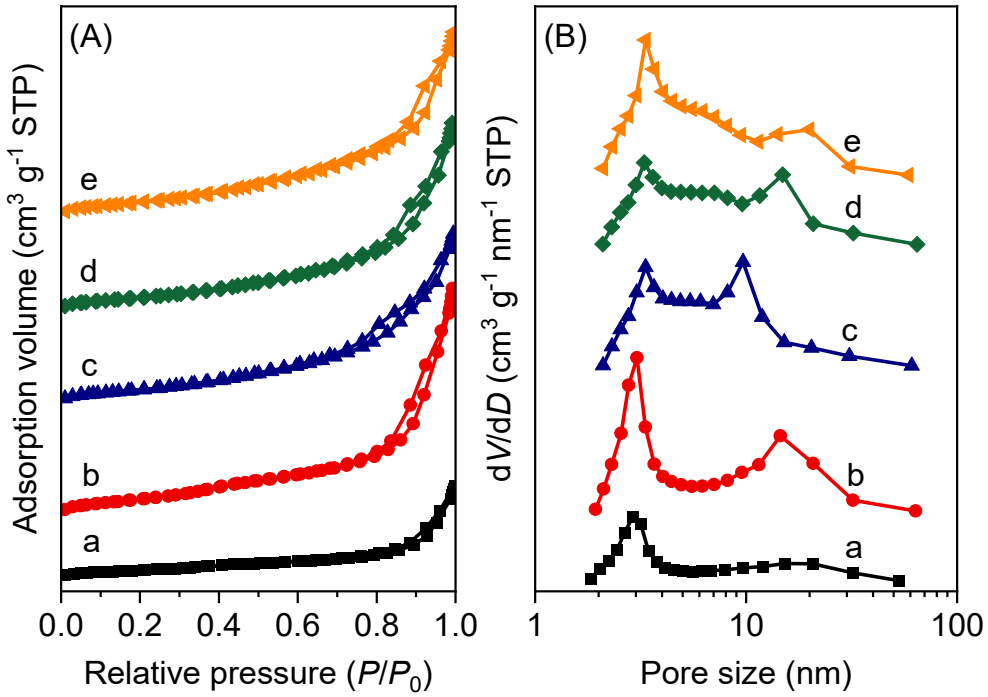


**Fig. S6** $N_2$ adsorption-desorption isotherms (A) and pore size distribution (B) of the as-calcined *x*CuPs/$CeO_2$ catalysts: (a) $x = 10$, (b) $x = 15$, (c) $x = 20$, (d) $x = 25$, (e) $x = 30$.

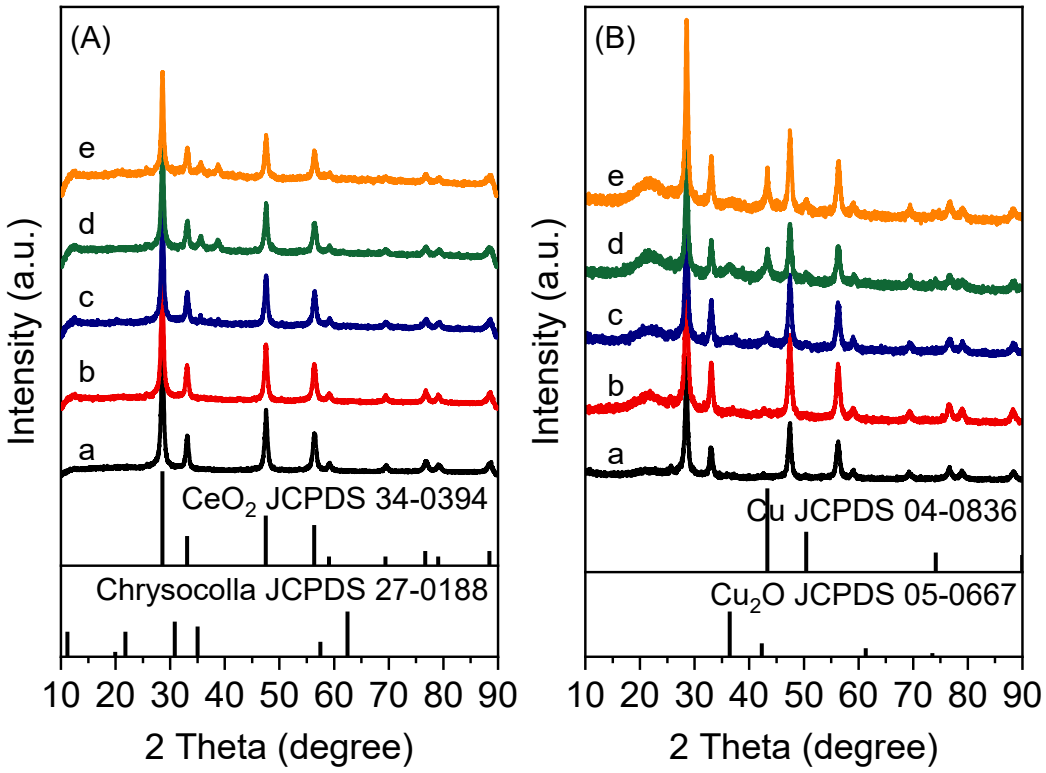


**Fig. S7** XRD patterns of the calcined (A) and reduced (B) *x*CuPs/$CeO_2$ catalysts: (a) $x = 10$, (b) $x = 15$, (c) $x = 20$, (d) $x = 25$, (e) $x = 30$.

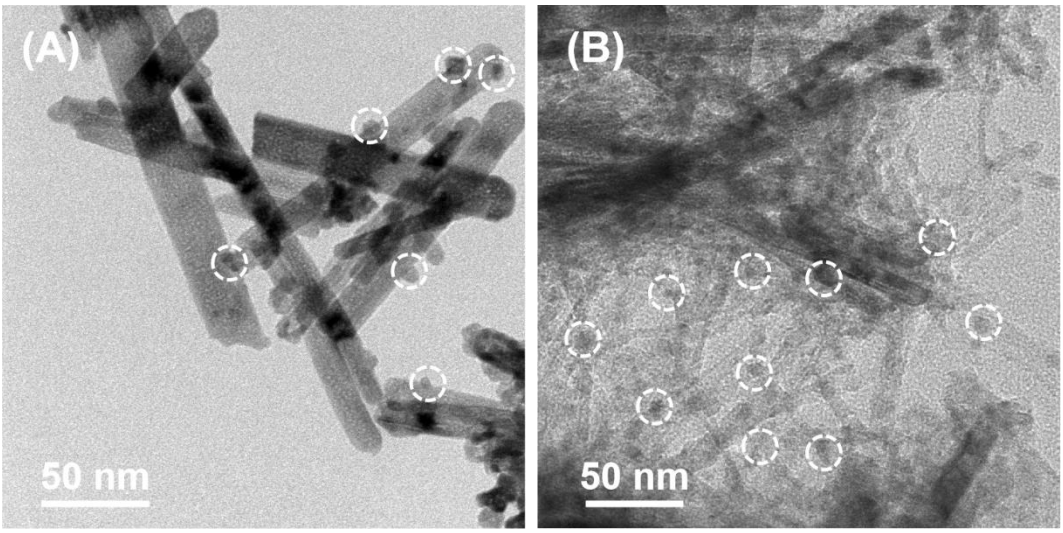


**Fig. S8** TEM images of the reduced Cu/$CeO_2$ and CuPs + $CeO_2$ catalysts

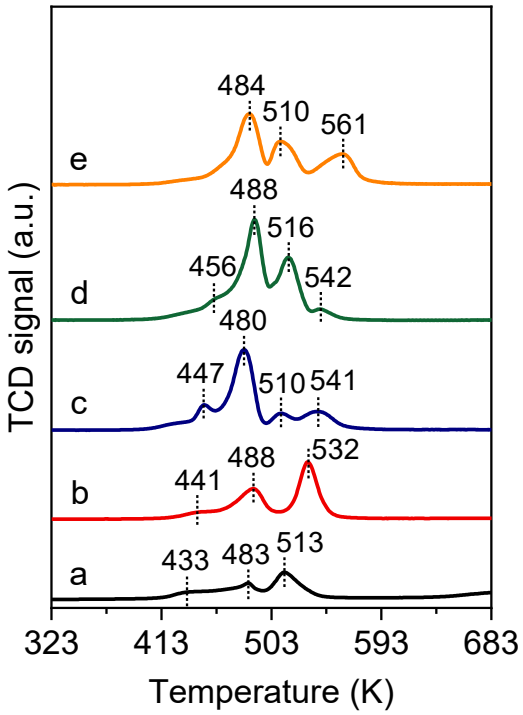


**Fig. S9** $H_2$-TPR profiles of the *x*CuPs/$CeO_2$ catalysts: (a) $x = 10$, (b) $x = 15$, (c) $x = 20$, (d) $x = 25$, (e) $x = 30$.

**Table S2** Physicochemical properties of the as-prepared Cu-based catalysts.

| Catalyst | [a] Cu loading (wt %) | $S_{BET}$ ($m^2\ g^{-1}$) | $V_{pore}$ ($cm^3\ g^{-1}$) | $D_{pore}$ (nm) | [b] $D_{Cu}$ (%) | [b] $S_{Cu}{}^0$ ($m^2\ g_{cat.}{}^{-1}$) |
|---|---|---|---|---|---|---|
| 10CuPs/$CeO_2$ | 9.1 | 156 | 0.58 | 13.8 | 34.2 | 20.2 |
| 15CuPs/$CeO_2$ | 14.1 | 367 | 1.44 | 13.1 | 39.9 | 36.5 |
| 20CuPs/$CeO_2$ | 22.7 | 330 | 1.09 | 10.6 | 34.3 | 45.5 |
| 25CuPs/$CeO_2$ | 26.3 | 309 | 1.20 | 12.4 | 26.9 | 48.6 |
| 30CuPs/$CeO_2$ | 27.8 | 346 | 1.19 | 10.9 | 19.8 | 33.8 |

[a] Cu loading calculated from ICP-OES.

[b] Cu dispersion and active surface area calculated from $N_2O$ titration.

**Table S3** XPS of the as-prepared *x*CuPs/$CeO_2$ catalyst.

| Entry | Catalyst | Atomic ratio (%) | | |
|---|---|---|---|---|
| | | $\frac{Cu^+}{Cu^+ + Cu^0}$ | $\frac{Ce^{3+}}{Ce^{3+} + Ce^{4+}}$ | O/Ce |
| 1 | 10CuPs/$CeO_2$ | 19.9 | 9.6 | 37.69 |
| 2 | 15CuPs/$CeO_2$ | 22.7 | 11.4 | 50.05 |
| 3 | 20CuPs/$CeO_2$ | 24.6 | 13.5 | 66.82 |
| 4 | 25CuPs/$CeO_2$ | 29.1 | 16.0 | 106.28 |
| 5 | 30CuPs/$CeO_2$ | 25.4 | 12.8 | 142.91 |

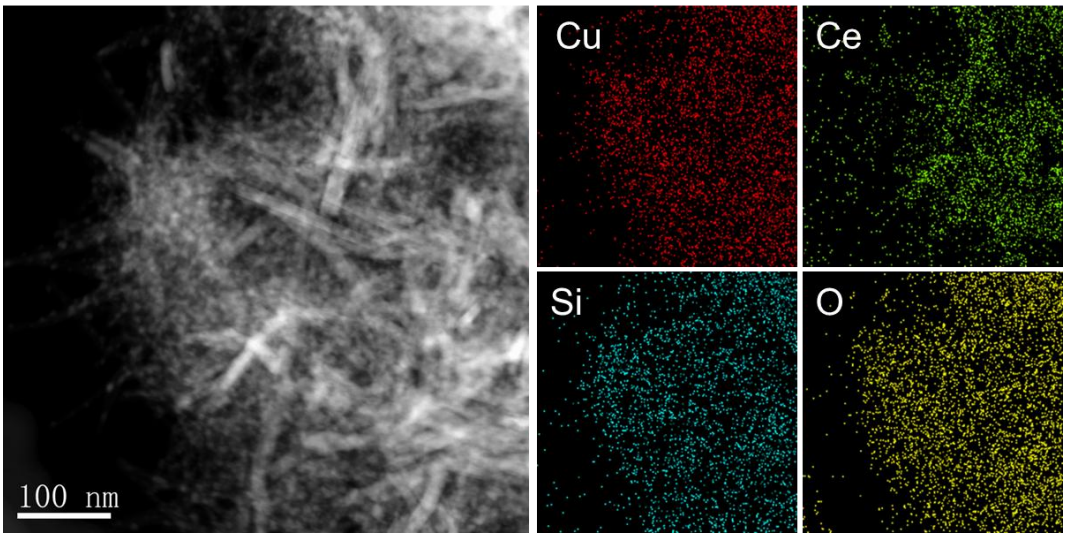


**Fig. S10** STEM image and element mapping of the reduced 25CuPs/$CeO_2$ catalyst

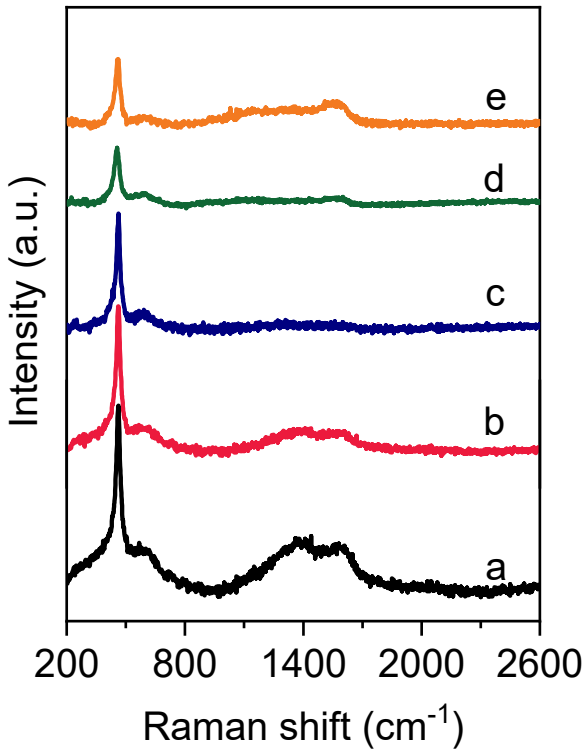


**Fig. S11** Raman shift of the as-calcined *x*CuPs/$CeO_2$ catalysts: (a) $x$ = 10, (b) $x$ = 15, (c) $x$ = 20, (d) $x$ = 25, (e) $x$ = 30.

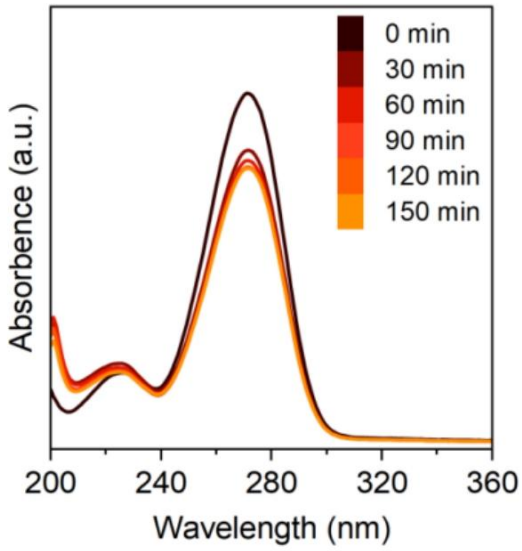


**Fig. S12** UV-vis spectra for the adsorption of furfural on the reduced 25CuPs/$CeO_2$ catalyst. Adsorption conditions: $C_{furfural}$ = 50 mM, $m_{cat.}$ = 50 mg, the Uv-vis spectra were collected per 30 min

The Uv-vis spectra was a viable alternative for probing the adsorption of FF on the catalyst surface. Accordingly, the reduced 25CuPs/$CeO_2$ was immersed in an FF solution under continuous stirring, and UV–vis spectra were recorded at 0.5 h intervals. The solution was subsequently separated by centrifugation to facilitate UV-vis spectra acquisition. As shown above, it was found that the residual FF decreased rapidly at initial 0.5 h stage and being stable gradually with the time prolonging, which revealed a strong interaction between the FF substrate and the 25CuPs/$CeO_2$ catalyst.

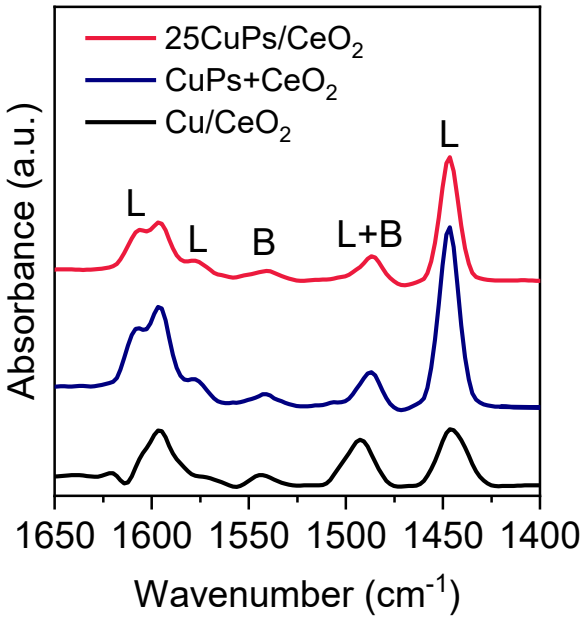


**Fig. S13** Py-IR spectra of the 25CuPs/$CeO_2$, CuPs+$CeO_2$, and Cu/$CeO_2$ catalysts desorbed at 298 K.

**Table S4** Acid properties of the as-prepared 25CuPs/$CeO_2$, CuPs+$CeO_2$, and Cu/$CeO_2$ catalysts at 298 K and 413 K.

| Entry | Catalyst | Temperature (K) | Acid sites (μmol $g^{-1}$) | | $n_B/n_L$ |
|---|---|---|---|---|---|
| | | | $n_B$ | $n_L$ | |
| 1 | 25CuPs/$CeO_2$ | 298 | 13.6 | 118.8 | 0.11 |
| 2 | Cu/$CeO_2$ | 298 | 15.8 | 78.1 | 0.20 |
| 3 | CuPs+$CeO_2$ | 298 | 16.5 | 181.0 | 0.09 |
| 4 | 25CuPs/$CeO_2$ | 413 | 7.9 | 63.1 | 0.13 |
| 5 | Cu/$CeO_2$ | 413 | 6.9 | 29.1 | 0.24 |
| 6 | CuPs+$CeO_2$ | 413 | 10.7 | 88.5 | 0.12 |

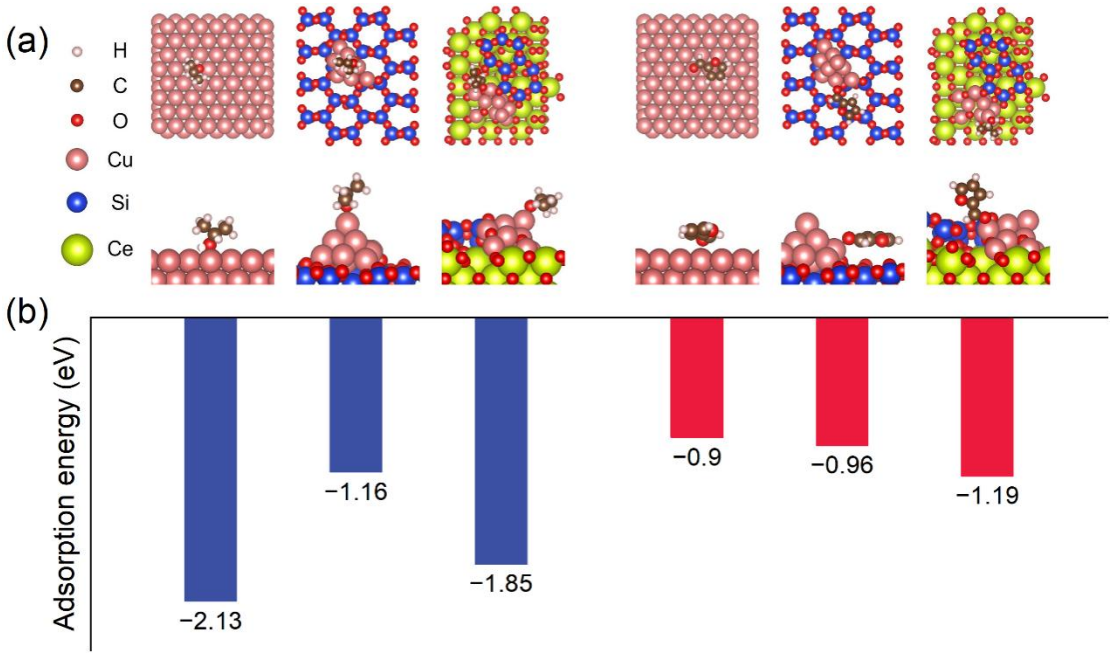


**Fig. S14** (a) adsorption configurations of *i*-PrOH and FF molecules on the structure models in top and side views: *i*-PrOH (left) and FF (right) adsorbed on Cu(111), Cu–O–Si, and Cu–O–Si/Ce, respectively. (b) adsorption energy of *i*-PrOH and FF molecules on the structure models.

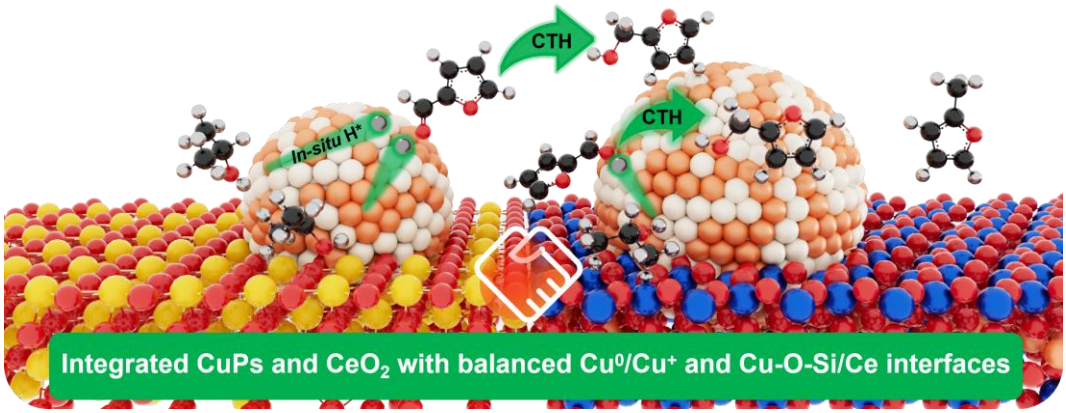


**Scheme S1** Illustration of CTH of FF to FOL on the integrated catalyst with balanced $Cu^0$ and $Cu^+$ dual sites.

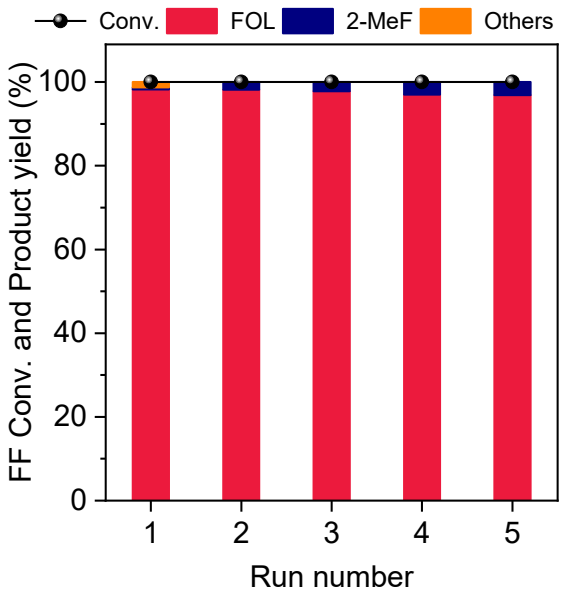


**Fig. S15** Catalytic stability evaluation for CTH of FF over the 25CuPs/$CeO_2$ catalyst. Reaction conditions: $m_{cat.}$ = 50 mg, $T$ = 413 K, $n$(FF) = 1 mmol, $V_{i\text{-PrOH}}$ = 20 mL, $P$(Ar) = 2 MPa.

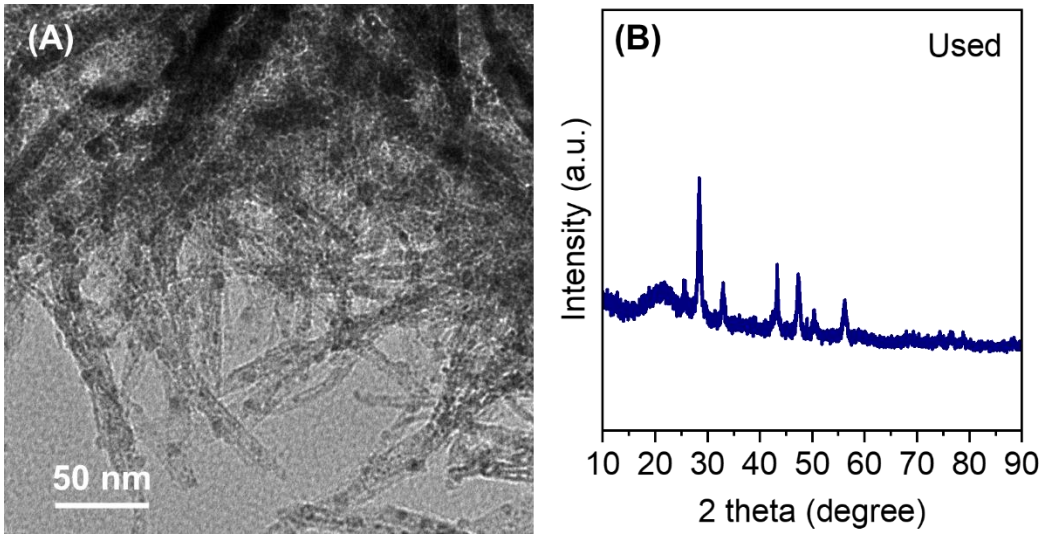


**Fig. S16** TEM image and XRD pattern of the used 25CuPs/$CeO_2$ catalyst

Contributing to the confinement of CuPs nanotube bundles and the cavity between CuPs and $CeO_2$, the Cu NPs could be observed with no obvious change in particle size. The XRD pattern could be index to the metallic Cu and $CeO_2$ phases, however, the diffraction intensity increased compared with the fresh catalyst. The Cu content did not change so much, further confirmed the stability of 25CuPs/$CeO_2$ catalyst. Thus, we speculated that the slightly decrease of catalytic performance might cause by the mass loss of catalyst between centrifugal separation rather than the structure damage.

## Notes and references


1 Y. Cui and W. Dai, *Catal. Sci. Technol.*, 2016, **6**, 7752–7762.

2 H. Li, Y. Cui, Y. Liu, S. Wang and W. Dai, *Nanotechnology*, 2022, **33**, 435703.

3 (a) G. Kresse and J. Furthmüller, *Comput. Mater. Sci.*, 1996, **6**, 15–50; (b) G. Kresse and J. Furthmüller, *Phys. Rev. B*, 1996, **54**, 11169–11186.

4 (a) J. P. Perdew, K. Burke and M. Ernzerhof, *Phys. Rev. Lett.*, 1996, **77**, 3865–3868; (b) J. P. Perdew, M. Ernzerhof and K. Burke, *J. Chem. Phys.*, 1996, **105**, 9982–9985.

5 (a) S. Grimme, J. Antony, S. Ehrlich and H. Krieg, *J. Chem. Phys.*, 2010, **132**, 154104; (b) S. Grimme, S. Ehrlich and L. Goerigk, *J. Comput. Chem.*, 2011, **32**, 1456–1465.

6 P. E. Blöchl, *Phys. Rev. B*, 1994, **50**, 17953–17979.

7 A. Hjorth Larsen, J. Jørgen Mortensen, J. Blomqvist, I. E. Castelli, R. Christensen, M. Dułak, J. Friis, M. N. Groves, B. Hammer, C. Hargus, E. D. Hermes, P. C. Jennings, P. Bjerre Jensen, J. Kermode, J. R. Kitchin, E. Leonhard Kolsbjerg, J. Kubal, K. Kaasbjerg, S. Lysgaard, J. Bergmann Maronsson, T. Maxson, T. Olsen, L. Pastewka, A. Peterson, C. Rostgaard, J. Schiøtz, O. Schütt, M. Strange, K. S. Thygesen, T. Vegge, L. Vilhelmsen, M. Walter, Z. Zeng and K. W. Jacobsen, *J. Phys.-Condes. Matter*, 2017, **29**, 273002.

8 K. Momma and F. Izumi, *J. Appl. Crystallogr.*, 2008, **41**, 653–658.

9 J. Wang, X. Ren, Q. Xiang, J. Jiang, F. Wang, Y. Guan, H. Xu and P. Wu, *J. Am. Chem. Soc.*, 2024, **146**, 18418–18426.